Observation of magnetospheric relativistic electrons accelerated by Pc-5 ULF waves

Lun C. Tan,[1,2] Shing F. Fung,[1] and Xi Shao[1,3]

Received 9 January 2004; revised 21 April 2004; accepted 26 April 2004; published 20 July 2004.

[1] Magnetic field, electric field and energetic electron measurements from CRRES, GOES-6 and -7 satellites are used to investigate the production of up to 2 MeV electron fluxes through a storm sudden commencement (SSC) event on August 27, 1991. Strong Pc-5 oscillations, whose electric field is mainly along the radial direction, and up to an order-of-magnitude enhancement in relativistic electron fluxes occurred simultaneously in a two-hour period. The enhanced electron fluxes are found to have a pancake-like pitch angle distribution, which is consistent with the fluxes being accelerated near the equatorial plane. The electron acceleration is shown to result from drift-resonant interactions with the toroidal-mode Pc-5 ULF waves having wave frequencies three times the electron drift frequency. In view of the L-variation of ULF wave frequencies, electron acceleration to relativistic energies becomes more effective in the geosynchronous region. *INDEX TERMS:* 2720 Magnetospheric Physics: Energetic particles, trapped; 2730 Magnetospheric Physics: Magnetosphere—inner; 2784 Magnetospheric Physics: Solar wind/magnetosphere interactions; 7807 Space Plasma Physics: Charged particle motion and acceleration; 7867 Space Plasma Physics: Wave/particle interactions. **Citation:** Tan, L. C., S. F. Fung, and X. Shao (2004), Observation of magnetospheric relativistic electrons accelerated by Pc-5 ULF waves, *Geophys. Res. Lett.*, *31*, L14802, doi:10.1029/2004GL019459.

1. Introduction

[2] Relativistic electrons in the radiation belts create a hazardous environment for space systems. The origin and acceleration of these electrons remain outstanding questions in radiation belt physics [e.g., *Fung*, 2004]. Recently, there has been increasing interest in the role of magnetospheric ULF waves (e.g., in the Pc-5 frequency range (1–10 mHz)) in enhancing relativistic (Mev) electron fluxes in the outer-belt zone. *Baker et al.* [1998] observed the correlation between the ground-magnetometer observations of ULF waves and the enhancements of MeV electron fluxes during two magnetic cloud events. Similar correlation over a 90-day period was also reported by *Rostoker et al.* [1998]. These studies indicate the coincidence of occurrence of ground-magnetic field oscillations in the Pc-5 frequency range and enhancement of magnetospheric relativistic electron fluxes. Since it is not straightforward to relate the ground-magnetic field perturbations to the magnetospheric electric fields that accelerate MeV-electron fluxes, these earlier studies did not lead to a determination of electron acceleration mechanism.

[3] *Hudson et al.* [1999] proposed that the electron acceleration could be due to a drift-resonant interaction with ULF waves. *Elkington et al.* [2003] further simulated the interaction of toroidal-mode (with radial electric field) and poloidal-mode (with azimuthal electric field) Pc-5 waves with azimuthally drifting electrons in a compressed dipole field. While the physics of wave-particle interaction may be elucidated from the simulation with simplified assumptions (e.g., globally propagating wave modes), it is important to verify the drift-resonant interaction observationally.

[4] On August 27 (Day 239), 1991, between 15.3–17.5 UT, an enhanced electron flux event was observed by CRRES, GOES-6 and -7 satellites near the geosynchronous region. The event featured up to an order-of-magnitude increase of MeV electron fluxes over a ~2 hour period. Strong electric field oscillations with frequencies of 2–4 mHz were observed during the electron flux enhancement period. In this letter we present the event analysis to demonstrate the role of Pc-5 waves in the acceleration of magnetospheric relativistic electrons.

2. Event Description

2.1. Inner Magnetosphere Satellite Constellation

[5] As shown in Figure 1, CRRES and GOES were on opposite sides of the Sun-Earth line, the spacecraft configuration is favorable for monitoring the dayside distribution of Pc-5 waves.

2.2. Solar Wind Conditions During the Event

[6] The event started with an initial magnetospheric compression at t_0 = 15.25 UT (the vertical dashed line in Figures 2 and 3), when a powerful (15A+7B+1C) storm sudden commencement (SSC) occurred (see http://www.wdcb.ru/stp/data/sudden.com/STORM2.SSC). The interplanetary magnetic field (IMF) and solar wind speed (V_{sw}) data as measured by the IMP-8 spacecraft are shown in bottom panel of Figure 2. Although the data are scarce, by averaging them over 13.0–14.4 UT and 15.3–17.0 UT respectively, we can still determine $V_{sw} = 320 \pm 10$ kms^{-1} and $P_{dyn} = 5 \pm 1$ nPa (*Pdyn* is the solar wind dynamic pressure) before SSC, and $V_{sw} = 450 \pm 20$ kms^{-1} and $P_{dyn} = 13 \pm 2$ nPa after SSC. During the event Kp was 6-, Dst was 8 nT, and AE increased from ~300 nT to 1500 nT (see 4th panel of Figure 2).

2.3. Characteristics of Observed Electron Flux Enhancements

[7] The CRRES Medium Energy A (MEA) spectrometer measured directional electron fluxes (J) in 17 energy

[1]Space Physics Data Facility, NASA/GSFC, Code 632, Greenbelt, Maryland, USA.
[2]QSS Group, Inc., NASA/GSFC, Code 633, Greenbelt, Maryland, USA.
[3]National Research Council, NASA/GSFC, Greenbelt, Maryland, USA.

0094-8276/04/2004GL019459

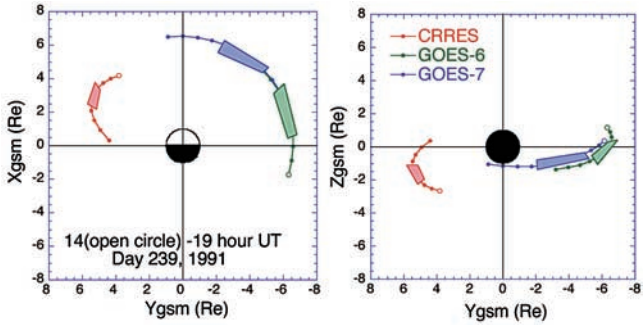

Figure 1. Orbits of CRRES, GOES-6 and -7 satellites at 14–19 UT, Day 239, 1991. In each orbit track an open circle marks the time of 14.0 UT, with each successive dot indicating a half-hour increment. The interval of electron flux enhancements is indicated by colored stripes.

channels covering the electron kinetic energy (T) range of 0.15–1.58 MeV [*Vampola*, 1996]. Fitting the pitch-angle (α) distribution of J to a $\sin^N \alpha$-function (i.e., $J = J_\perp \sin^N \alpha$) by using the flux data sampled in the α range of 30°–150° within one minute, we calculate the anisotropy index (N) and the local perpendicular flux ($J_\perp$) at α = 90°. Since during the period of enhanced electron fluxes $\langle B/B_{min} \rangle = 1.02 \pm 0.02$, where B and B_{min} are respectively the local magnetic field and minimum field along the same field line, $J_\perp$ also expresses the equatorial perpendicular flux.

[8] When the initial compression occurred (see 5th panel of Figure 2), $J_\perp$ (CRRES) showed a sharp decrease, which was more pronounced at higher energies. Afterwards, $J_\perp$ went through a series of oscillations and its overall level began to increase. The enhancement of $J_\perp$ is more pronounced at middle energies (~0.8 MeV). The energy dispersion of J oscillations indicates their drift-echo origin, which will be verified by the drift period analysis later. Multiple peaks are also seen in N (CRRES) (see 3rd panel of Figure 2) with some peak-N values reaching as high as 7. We note that the N-peaks coincide with the $J_\perp$-peaks at the same T channel, implying that the enhancement in electron fluxes are predominantly due to the increase in electrons with $\alpha \sim 90°$, i.e., they may be locally accelerated near the equatorial plane.

[9] We also show the mean fluxes J_{av} (1.5 MeV) (CRRES) and J_{av} (>2 MeV)(GOES) in 2nd panel of Figure 2. Because of the difference in L location and $J_\perp$ definition between CRRES and GOES (see http://spidr.ngdc.noaa.gov/spidr/), the two fluxes are not directly comparable. Nevertheless, their general trends are similar, indicating that the electron flux at $T \sim 2$ MeV can increase by an order of magnitude within ~2 hours.

2.4. Characteristics of ULF Wave Observations

[10] Hereafter we exhibit the electric field (**E**) and magnetic field (**B**) measurements in the cylindrical system (ρ, ϕ, z), in which $\hat{\rho}$ points radially outward, $\hat{\phi}$ points counterclockwise with $\phi = 0$ being along the sunward direction, and $\hat{z}$ points northward. The CRRES **E** and **B** data (see http://crres.bu.edu/crres.html) are shown in 4th and 5th panels of Figure 2, respectively. During the period of enhanced electron fluxes there were strong ULF electric field oscillations whose average value was ~0. The periods (τ_w) of oscillations were ~4.3 and ~3.2 (min) at 15.5 and 17.0 UT, respectively. The largest oscillation was along the radial direction (E_ρ), consistent with the toroidal-mode Pc-5 waves [*Elkington et al.*, 2003]. In addition to **E** waves, weak **B** waves were superposed on the compressed background field, which had the largest enhancement along the z-direction. Note that here **B** is presented by subtracting the Olson and Pfitzer model field adopted by CRRES. Thus Figure 2 clearly shows the correlation between ULF wave generation and magnetic compression. In fact, the waves disappeared after 17.5 UT when the compression vanished (i.e., B_z(CRRES)-B_z(model) ~0).

2.5. Comparison of Magnetic Field Measurements Between CRRES and GOES

[11] From B_z data shown in Figure 3 it is seen that the maximum magnetospheric compression occurred near the Sun-Earth line, as indicated by nearly the same enhancements of the main field component (B_z) seen by both CRRES and GOES-7, and a smaller enhancement seen by GOES-6 close to dawn.

[12] Since no electric field data were available in the dawn flank, from B_ϕ measurements by GOES we infer E_ρ information there. For standing Alfven waves on the ambient geomagnetic field line, we expect a 90° phase shift between the disturbance field components δB_ϕ and δE_ρ with

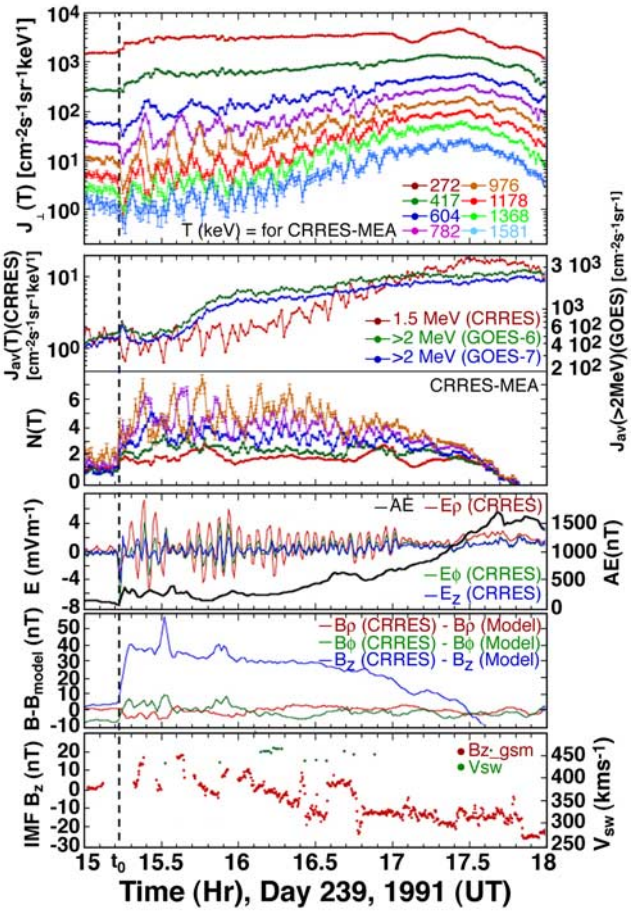

Figure 2. Time profiles of electron flux and anisotropy, magnetic and electric field observed by CRRES, and solar wind data.

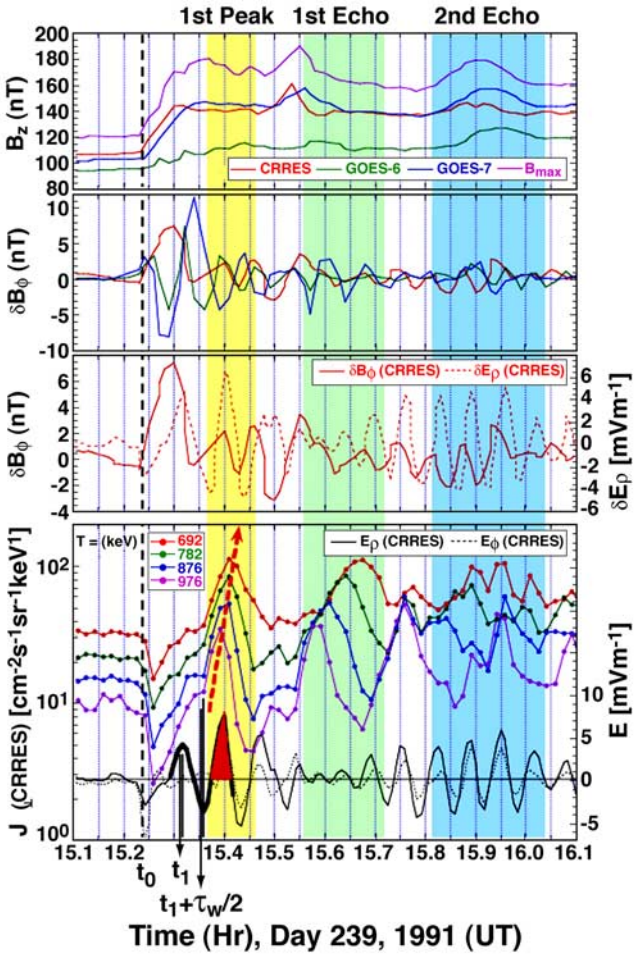

Figure 3. Time profiles of electron flux, magnetic and electric field data during the first hour after SSC.

δB_ϕ leading δE_ρ [*Nakamura et al.*, 1994]. δB_ϕ and δE_ρ measured by CRRES are shown in 3rd panel of Figure 3. The phase shift between δB_ϕ and δE_ρ(δB_ϕ leading δE_ρ by $\sim$1/4 τ_w) is clearly seen, particularly in the well-developed wave region denoted by "2nd echo". Since in 2nd panel of Figure 3 the phase of δB_ϕ in the dawn flank (as measured by GOES) was opposite to that in the dusk flank (as measured by CRRES), the phase of (E_ρ $\sim\delta E_\rho$, as $\langle E_\rho \rangle \sim 0$) in the dawn flank should also be opposite to that in the dusk flank (as measured by CRRES). This key information will be used in the discussion on resonant acceleration.

3. Discussion and Summary

3.1. Compressed Dipole Field Model

[13] Results from our study are consistent with *Elkington et al.* [2003] that the resonant interaction between the radial motions of electron guiding centers along their drift orbits in

Table 1. E_ρ Sign and Electron Acceleration

Flank	Dawn		Dusk	
$\Delta\rho$	>0		<0	
E_ρ	>0	<0	>0	<0
Acceleration	No	Yes	Yes	No

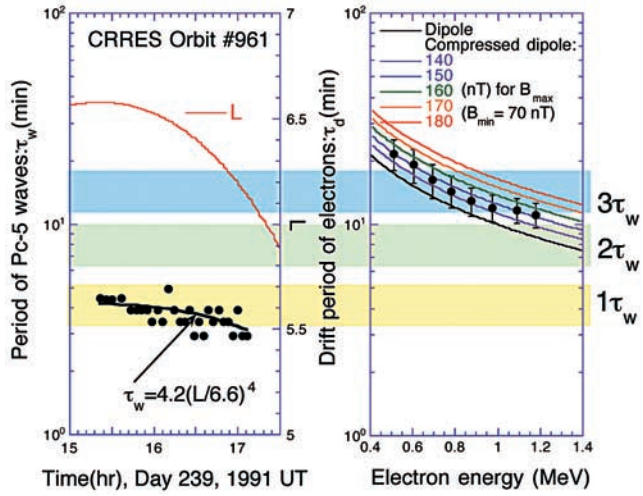

Figure 4. (left) The observed wave period τ_w vs. time, or CRRES positions in L; (right) the observed drift period τ_d vs. electron energy. The color stripes show regions of $1\tau_w$, $2\tau_w$ and $3\tau_w$ during the first hour after SSC.

a day-night asymmetric magnetospheric magnetic field and the toroidal ULF waves can cause electron accelerations. Their assumption of constant-amplitude ULF waves propagating globally, however, is over-simplified and is not supported by observations. It is known [e.g., *Rostoker et al.*, 1998] that the power of Pc-5 waves is concentrated in both dawn and dusk flanks, particularly in the dawn-noon sector. According to the estimation of *Li et al.* [1993] also, the wave amplitude in the night side is expected to be less than that in the dayside by one order of magnitude. Therefore, electron acceleration should only occur in the dayside (see the blue and red bands in the upper right panel of Figure 5) when the electron energy gain $\delta T(= -e\langle E_\rho \rangle \Delta\rho) > 0$ (e is the electron charge) due to the opposite signs of $\langle E_\rho \rangle$ and $\Delta\rho$ (see Table 1). In the night-side electrons only execute drift motions without any energy change.

[14] *Elkington et al.* [2003] introduced a compressed dipole field,

$$B(\rho, \phi) = b_0 + b_1(1 + b_2 \cos\phi), \tag{1}$$

where $b_0 = B_0 R_e^3/\rho^3$(B_0 = 3.11 $\times$ 10^4 nT), b_1 and b_2 are estimated from GOES observations. In addition, instead of b_1 and b_2 we take $B_{max} = b_0 + b_1$ (1 + b_2) (see 1st panel of Figure 3) and $B_{min} = b_0 + b_1$ (1 $-$ b_2) ($\sim$70 nT) as model parameters.

[15] In the absence of any perturbing forces, the guiding centers of equatorially trapped electrons drift along constant-B contours. The time interval during which an electron drifts from ϕ_1 to ϕ_2 is

$$\Delta t_d(\phi_1, \phi_2) = \left(\gamma e L_d^2 R_e^2/3Mc\right)\left(1 + b_1 L_d^3/B_0\right) \cdot \int_{\phi_1}^{\phi_2} \left(1 - b_1 b_2 L_d^3 \cos\phi/B_0\right)^{-5/3} d\phi, \tag{2}$$

where L_d is ρ value of electron drift orbit at dawn (or dusk), $M = p^2/2m_0B$ is the relativistic first adiabatic invariant, γ is the relativistic correction factor, c is the light speed, and m_0

and p are the mass and momentum of electrons, respectively.

[16] To test equation (2), we compare the electron drift period τ_d calculated from it (i.e., $\tau_d = \Delta t_d$ (0, 2π)) to that deduced from drift echo analysis. For valid comparison, however, we need to find a time interval during which there are negligible perturbing forces (e.g., $E_\rho \sim 0$). Since such interval does not exist, we have to take the minimum E_ρ interval between "1st peak" and "1st echo" (see Figure 3) for our purpose. As shown in Figure 4, the observed τ_d is systematically higher than that predicted for the dipole field model (i.e., $b_1 = 0$ in equation (2)), which is due to magnetospheric compression [*Elkington et al.*, 2003]. Also, the observed τ_d is more consistent with the compression dipole field model with $B_{max} = 150$ (nT), although the observed B_{max} is ~170 (nT).

[17] In Figure 4 the decrease of τ_w with time corresponds to a decrease of field line lengths at smaller L coordinates of CRRES. In fact, $\tau_w \propto L^{(4\ \pm 1)}$ as given by *Singer and Kivelson* [1979] is consistent with our observations. Also, we find $\tau_d = 3\tau_w$ for the main enhancement of $J_\perp$ around $T \sim 0.8$ MeV.

3.2. Acceleration of Electron Fluxes in Their First Peak

[18] In order to explore the details of electron acceleration, we plot $J_\perp$ of selected T channels, E_ρ and E_ϕ in bottom panel of Figure 3. The sharp decrease of $J_\perp$ immediately after t_0 can be related to the acceleration due to the large negative spike of E_ϕ(CRRES). In fact, $E_\phi < 0$ means $\Delta T(= -2\pi\, e\langle E_\phi\rangle \rho \Delta\tau_w/\tau_d) > 0$, where $\Delta\tau_w \sim 2$ (min) is the width of E_ϕ pulse. Because of the conservation of M, the accelerated electrons will have to move to a smaller L region. Thus CRRES at $L \sim 6.6$ would observe the electrons originating at a higher L, and detect a lower $J_\perp$ because of the negative L-gradient of $J_\perp$. As T increases τ_d decreases and ΔT increases, the decreases of $J_\perp$ should be more pronounced at higher energies (see Figure 2).

[19] After t_0 the electron acceleration by E_ρ became a dominant effect. During the first $E_\rho > 0$ half-period, however, $J_\perp$ only recovered to its pre-SSC level. The first peak of $J_\perp$ corresponds to the second $E_\rho > 0$ half-period (the "red peak" in Figure 3). We note that the arrival time t_p of $J_\perp$ peaks is a decreasing function of T (indicated by the red arrow). Based on equation (2) we have $t_p(T) - t_i(T) = \Delta t_d(\phi_i(T), \phi_{CRRES})$, where ϕ_i is the azimuth of $J_\perp$ peak at time t_i. We then calculate ϕ_i at given t_i. By varying t_i we find that when $t_i = t_1$ (the time of the first $E_\rho > 0$ peak, see Figure 3) the ϕ_i values of all seven T channels between 0.60 and 1.18 MeV are at the same ϕ_1 (the standard deviation $\sigma(\phi_i) \sim 3°$), indicating the formation of an electron bunch. Taking into account of $\sigma(t_1) \sim 0.5$ (min), we obtain $\langle\phi_1\rangle = -30 \pm 10°$ at t_1. Thus the bunch should be created by the $E_\rho < 0$ half-period earlier in the dawn-noon sector. In addition, since CRRES ($\phi_{CRRES} = 53°$) began to detect the first electron bunch at $t_i = t_1 + \tau_w/2$, when the $J_\perp$ peak was still at $\phi = 13 \pm 9°$, the half-width of electron azimuthal extension is ~π/4 (i.e., the width of electron acceleration region ~π/2).

[20] From the observations presented above a scenario of electron acceleration by toroidal electric field E_ρ is shown in Figure 5. Because of $\tau_d = 3\tau_w$ an electron located at A ($\phi \sim -\pi/3$) at t_1 should be at B ($\phi \sim 0$) at $t_1 + \tau_w/2$, and at C ($\phi \sim$ π/3) at $t_1 + \tau_w$. First at A (in the dawn-noon sector) the $E_\rho < 0$ half-period (the "blue dip") causes electron acceleration. Then the accelerated electron passed B without energy change because of $E_\rho \sim 0$ (E_ρ changes its polarity between dawn and dusk). Finally, at C (i.e., near CRRES) the $E_\rho > 0$ half-period (the "red peak") further accelerates the electron. As a result, the electron undergoes accelerations twice by E_ρ as it drifts from A to C. In addition, our observation shows (not given here) that the poloidal electric field E_ϕ also undergoes a phase reversal between dawn and dusk. Thus an electron accelerated at A when $E_\phi < 0$ will encounter a deceleration field $E_\phi > 0$ at C after drifting for a τ_w, leading to a zero net gain of electron energy by E_ϕ.

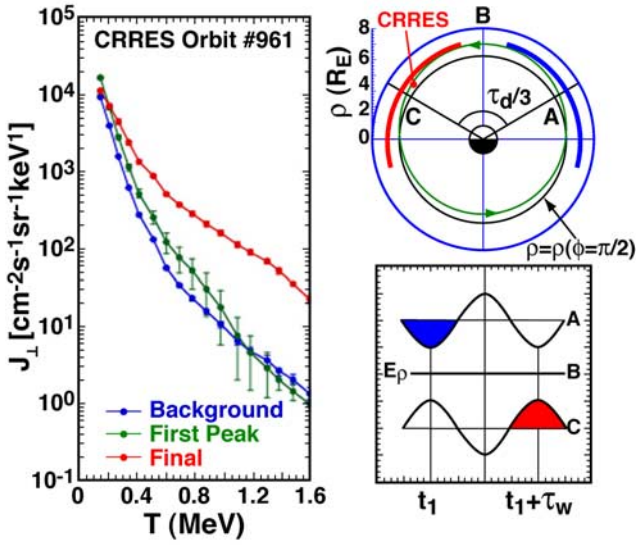

Figure 5. (left) The background (sampled in 15.0–15.2 UT), first-peak (sampled in 15.35–15.45 UT) and final (sampled in 17.3–17.5 UT) $J_\perp$ spectra; (right) the suggested scenario of electron acceleration (upper) and the waveforms of E_ρ (lower). Here the green line is the drift path of equatorially trapped electrons encountered by CRRES.

[21] Therefore, the first $J_\perp$ peak should be energized by the E_ρ segment denoted by the thickened line in Figure 3. Note that this segment corresponds to the waveform C in Figure 5. By comparing the first-peak $J_\perp$ spectrum with the pre-SSC background spectrum in Figure 5, we note that ΔT maximizes in the middle energy range, with $\Delta T \sim 0.12$ MeV at $T \sim 0.8$ MeV. This value can be checked against the predicted gain $\Delta T = -2e\langle E_\rho\rangle\Delta\rho$ (here the factor 2 expresses continuous acceleration in both flanks). With $\langle E_\rho\rangle \sim 6\text{m Vm}^{-1}$ (see the "red peak" in Figure 3) and $\Delta\rho \sim 1.2\ R_e$ [see *Elkington et al.*, 2003], we obtain $\Delta T \sim 0.09$ MeV.

3.3. Continuous Enhancement of Electron Flux for ~2 Hours

[22] It is obvious that in Figure 3 each E_ρ segment similar to the waveform C in Figure 5 can accelerate electrons. Therefore, the clear display of energy-dispersed echoes in the "1st echo" region is due to the absence of newly accelerated electrons there because of $E_\rho \sim 0$. Also, the recovery of E_ρ waves in the "2nd echo" region can account for the correspondence of peaks between E_ρ and $J_\perp$. Thus $J_\perp$ can reach its final spectrum within ~2 hours.

[23] Continuous acceleration of electrons is possible only if the drift-resonance condition $\tau_w = \tau_d/3$ is maintainedcontinuously. In order to conserve the first adiabatic invariant M, the accelerated electron should move inward to a higher B or lower L region. In a dipole field, equation (2) yields $\tau_d \propto L^2$ at constant M by setting b_1 to zero. In a compressed dipole field, however, τ_d should be evaluated numerically. In view of the standoff distance of the magnetopause at the subsolar point ($\sim$7.7 R_e), we have calculated τ_d below $L = 8$ and determined the following net L-dependence of τ_d: $\tau_d \propto L^{2.2}$ at $L = 4-6$, and $\tau_d \propto L^{3.8}$ at $L = 6-8$. Since it has been found that Pc-5 wave periods depend on L as $\tau_w \propto L^{(4 \pm 1)}$ [*Singer and Kivelson*, 1979], we conclude that $\tau_w = \tau_d/3$ can be satisfied fairly continuously only at $L > 6$. This simple fact may largely be responsible for the enhancements of relativistic electrons seen near the geosynchronous region [*Li et al.*, 1997].

[24] In summary, since Pc-5 waves widely exist during magnetospheric storm or substorm activities, particularly in the dawn and dusk flanks, observations presented in this letter support relativistic electron acceleration by the drift-resonant interaction with Pc-5 waves.

[25] **Acknowledgments.** The authors thank A. L. Vampola for archiving the CRRES-MEA data at the National Space Science Data Center. This work was partially supported by NASA contract NAS 5-97059 and NASA RTOP 784-50-51-02.

References

Baker, D. N., et al. (1998), Coronal mass ejections, magnetic clouds, and relativistic magnetospheric electron events: ISTP, *J. Geophys. Res.*, *103*(A8), 17,279–17,292.

Elkington, S. R., et al. (2003), Resonant acceleration and diffusion of outer zone electrons in an asymmetric geomagnetic field, *J. Geophys. Res.*, *108*(A3), 1116, doi:10.1029/2001JA009202.

Fung, S. F. (2004), Survey of current situation in radiation belt modeling, *Adv. Space Res.*, in press.

Hudson, M. K., et al. (1999), Simulation of radiation belt dynamics driven by solar wind variations, in *Sun-Earth Plasma Connections*, edited by J. L. Burch et al., *Geophys. Monogr. Ser. AGU*, vol. 109, p. 171–182, AGU, Washington D. C.

Li, X., et al. (1993), Simulation of the prompt energization and transport of radiation belt particles during the March 24, 1991 SSC, *Geophys. Res. Lett.*, *20*(22), 2423–2426.

Li, X., et al. (1997), Mutisatellite observations of the outer zone electron variations during the November 3–4, 1993 magnetic storm, *J. Geophys. Res.*, *102*(A7), 14,123–14,140.

Nakamura, M., et al. (1994), Pc5 pulsations observed in the dayside magnetosphere by Geotail, *Geophys. Res. Lett.*, *21*(25), 2903–2906.

Rostoker, G., et al. (1998), On the origin of relativistic electrons in the magnetosphere associated with some geomagnetic storms, *Geophys. Rev. Lett.*, *25*(19), 3701–3704.

Singer, H. J., and M. G. Kivelson (1979), The latitudinal structure of Pc 5 waves in space: Magnetic and electric field observations, *J. Geophys. Res.*, *84*, 7213–7222.

Vampola, A. L. (1996), The ESA outer zone electron model update, in *Proc. on Environment Modeling for Space-based Applications*, ESTEC, Noordwijk, NL, 18–20, September.

L. C. Tan, S. F. Fung, and X. Shao, NASA/GSFC, Code 632, Greenbelt, MD 20771, USA. (ltan@pop600.gsfc.nasa.gov; fung@mail630.gsfc.nasa.gov; shao@mail630.gsfc.nasa.gov)